PERGAMON

International Journal of Heat and Mass Transfer 43 (2000) 1837–1849

International Journal of HEAT and MASS TRANSFER

www.elsevier.com/locate/ijhmt

Experimental verification of the role of Brinkman number in microchannels using local parameters

C.P. Tso*, S.P. Mahulikar

School of Mechanical and Production Engineering, Nanyang Technological University, Nanyang Avenue, Singapore 639798, Singapore

Received 4 January 1999; received in revised form 15 July 1999

Abstract

Experiments were performed using water flow in microchannel specimens, with thermocouples mounted axially along the flow for local wall temperature measurement. The processed experimental data obtained locally in the laminar regime exhibited the unusual behaviour of the local Nusselt number decreasing with increasing local Reynolds number along the flow. Though the variation of Nusselt number with Reynolds number has been observed before, it was for averaged parameters, obtained using a different approach in experimentation for calculating these parameters over the entire microchannel specimen. The present experimental data in the laminar regime were also found to correlate well with the Brinkman number for the individual sets and much better globally, by combining all the data sets. The correlation with the Brinkman number in spite of its relatively low values is physically interpreted.

Keywords: Brinkman number; Flow transitions; Forced convection; Microchannel cooling; Temperature-dependent properties

1. Introduction

Microchannel cooling using liquid coolant is seriously considered for the cooling of the next generation integrated circuit (IC) chips, since it offers much reduced thermal resistance of the fluid boundary layer. Hence, the behaviour of single-phase forced-flow convection in microchannels has been extensively investigated, especially experimentally, and the behaviour was reported to deviate significantly from that in the conventionally-sized channels.

Peng and Wang [1] experimentally investigated the forced convection characteristics of water flowing through microchannels with a cross-section of 0.6×0.7 mm, machined on a 2 mm thick stainless steel plate. Thermocouples for measuring the liquid temperature, T_f, were located at the inlet and outlet of their test section with six thermocouples mounted on the back of the microchannel plate. The convective heat transfer coefficient, h, thus obtained, was representative of the entire section, and varying the applied heat flux, $\dot{q}''_w$, for a specified condition of liquid velocity, V_m, and subcooling, simulated the axial variation of T_f and other parameters. The variation of the Nusselt number, Nu, with the Reynolds number, Re, exhibited the unusual behaviour of Nu decreasing with increasing Re, since for the conventionally-sized channels, the average Nu should increase with increase in average Re over the length, due to Nu increase in the thermal entry length. They have compared their experimental data for microchannels in the laminar regime with the correlation for the conventionally-sized channels with viscosity variation, viz., the Sieder–Tate equation [2], and

* Corresponding author. Tel.: +65-799-5033; fax: +65-791-1859.

E-mail address: mcptso@ntu.edu.sg (C.P. Tso).

0017-9310/00/$ - see front matter
PII: S0017-9310(99)00241-0

Nomenclature

Br	Brinkman number $=(\mu \times V_m^2)/(k \times \Delta T)$
$C_{H,I}$	empirical constant in Eq. (1.1)
C_p	specific heat of coolant (J/kg K)
D_h	hydraulic diameter of microchannel (m)
h	forced convective heat transfer coefficient (W/m^2 K)
$\bar{h}$	average forced convective heat transfer coefficient from Eq. (5) (W/m^2 K)
H	height of rectangular microchannel (m)
k	thermal conductivity of coolant (W/m K)
L	length of test specimen (m)
$\dot{m}$	coolant mass flow rate in microchannel (kg/s)
Nu	Nusselt number $(=hD_h/k)$
Pr	Prandtl number $(=\mu C_p/k)$
$\dot{q}''_w$	constant wall heat flux supplied to microchannel coolant (W/m^2)
Re	Reynolds number $(=V_m D_h/\nu)$
t	thickness of test specimen (m)
T	temperature (K)
ΔT	wall–fluid temperature difference (K)
V	velocity of coolant (m/s)
W	width of rectangular microchannel/width of test specimen (m)
W_{cn}	shortest distance between two consecutive microchannels (m) (cf. Fig. 1)
x	axial location in microchannel measured from inlet (m)

Greek

μ	dynamic viscosity (N s/m^2)
ν	kinematic viscosity (m^2/s)
σ	standard deviation

Subscripts

bk	back face of test specimen
ex	exit of microchannels
f	liquid coolant flowing through microchannel
fr	front face of test specimen
in	inlet of microchannels
lm	laminar
m	mean
tr	transition
w	wall of microchannel
1, 2	referring to test specimen 1, 2

the correlation for microchannels for $Re > 3000$, proposed by Wu and Little [3]. However, the Sieder–Tate equation shown in their Fig. 6 predicts the parameter, $Nu/Pr^{1/3}$, to increase with increase in Re, which is not representative of the unusual behaviour of convective heat transfer in the laminar regime in microchannels, discussed later. Hence, their experimental data for low values of Re shown in their Fig. 6 do not seem to qualitatively agree with their Eq. (4) (which is the same as the Sieder–Tate equation [2]). The correlation proposed by Wu and Little [3] does not seem to agree in trend with the experimental data for low values of Re, as seen in Fig. 7 [1].

Peng et al. [4] have experimentally investigated the forced-convection of water through rectangular microchannels having hydraulic diameter, D_h, in the range 0.133–0.367 mm, and aspect ratio, H/W, in the range 0.333–1. A representative h was calculated based on the downstream end of the microchannel, defined as

$$h = \dot{q}''_w/(T_w - T_{f,in}), \tag{1}$$

where T_w is assessed to be the value measured at the downstream end. Their data in their Figs. 3–6(b) indicate the unusual behaviour of $Nu/Pr^{1/3}$ decreasing with increasing Re, though they have not explicitly mentioned it. They have compared their data in the laminar regime with the Sieder–Tate equation [2]. Since the Sieder–Tate equation did not correlate well quantitatively with their experimental data, they have proposed a new correlation, viz.,

$$Nu = C_{H,I} \times Re^{0.62} \times Pr^{1/3}, \tag{1.1}$$

where $C_{H,I}$ is an empirical constant that depends on the geometric configuration of the microchannels. They compared Eq. (1.1) with their experimental data. However, neither Eq. (1.1) nor the Sieder–Tate equation, qualitatively agree with the unusual behaviour exhibited by their experimental data.

Wang and Peng [5] have experimentally investigated the single-phase forced-flow convection of water and methanol in microchannels. The h was evaluated as in Eq. (1) at the downstream end of the microchannels, where T_w was determined from the three measurements at the same axial location along the flow direction. Based on their experimental results, they have reported the unusual behaviour of Nu decreasing with increasing Re in the laminar regime, and an approximately constant Nu in the transition regime. The change from laminar flow to transition flow in microchannels was found to depend on T_f and V_m.

Peng and Peterson [6] have conducted experiments with different microchannels to examine the single-phase forced convective heat transfer and flow characteristics. The h was evaluated as in Eq. (1). The re-

lation of *Nu* with *Re* was found to be complicated in the transition and laminar regimes. In these regions, *Nu* was reported to decrease with an increase in *Re*, and *Nu* exhibited dependence on other factors like T_f and V_m. The transitions were also found to be influenced by T_f and V_m. In another paper [7], they have experimentally investigated the single-phase forced convective heat transfer and flow characteristics of water in microchannel structure plates with rectangular cross-section microchannels having a D_h of 0.133–0.367 mm. Due to significant variations in T_f, *Re* varies along the length of the microchannel. However, the liquid viscosity at the inlet was used to calculate *Re*. The *h* was evaluated as

$$h = \dot{q}''_w/T_m, \tag{2}$$

where ΔT_m is the log–mean wall–fluid temperature difference defined as

$$\Delta T_m = \frac{\Delta T_{in} - \Delta T_{ex}}{\ln(\Delta T_{in}/\Delta T_{ex})}. \tag{2.1}$$

Since ΔT_m is unique for the entire length of the microchannel, *h*, *Nu* and *Re* were again representative of the entire microchannel plate. However, from their experimental data points shown in their Fig. 2, it can be inferred that the unusual behaviour exists for fixed microchannel geometry in the laminar regime, which is not reflected by their proposed correlation in the laminar regime, viz., their Eq. (8).

Mala et al. [8] numerically investigated the possible importance of the electric double layer (EDL) at the solid–liquid interface, on the convection and liquid flow in microchannels. They found that the EDL modifies the velocity profile and reduces the average velocity, thereby increasing the pressure drop and reducing the heat transfer. In their Fig. 9, the local *Nu* reduces due to the EDL, by comparing the *Nu* values without EDL. However, in their Fig. 10, Nu_m (average taken over the length) increases with *Re*, with the effect of EDL, which does not agree with the experimentally observed unusual behaviour of *Nu* decreasing with increasing *Re*. In their Fig. 8, they have shown the temperature profiles along the length for a fixed *Re*, which suggests that they have not incorporated the variation of *Re* along the flow due to variation of T_f, which is responsible for the unusual behaviour as discussed later in this paper. Also, they reported that the EDL thickness ranges from a few nanometers to several hundreds of nanometers, and have calculated the effect on a microchannel separation distance of 25 μm. As this is an order of magnitude smaller than the channels used in the reported experimental investigations, the true influence of EDL on convection is uncertain.

Tso and Mahulikar [9] have shown the experimental data in the laminar regime reported in [5] to correlate with the Brinkman number, *Br*, in addition to *Re*, *Pr*, and a dimensionless geometric parameter of the microchannels, thereby explaining the unusual behaviour. In another paper [10], they have shown *Br* to determine the flow regime boundaries from laminar-to-transition and transition-to-turbulent, in addition to *Re* and a dimensionless geometric parameter of the microchannels, by analysing the experimental data reported in Ref. [5]. The reported unusual behaviour on flow transitions and transition range were also explained. In Ref. [11], they have analysed the data reported in Ref. [5] and also some of the data obtained from the present investigation. They showed that the unusual behaviour of *Nu* decreasing with increasing *Re* for the case of the fluid heated as in microchannel cooling of ICs, is not merely a characteristic of a thermally-developing flow in microchannels.

In summary, experiments have been reported in which *h* is representative of the entire length of the microchannels, calculated either at the downstream end of the microchannels or based on the bulk mean wall–fluid temperature difference over the entire length of the microchannels. The unusual behaviour of *Nu* decreasing with increasing *Re* is observed in the laminar regime. Though correlations for convection in the laminar regime have been reported [1,4,7], they do not agree in trend with most of the reported experimental data. However, experiments have not been reported in which T_w is measured axially along the flow, in order to calculate the local *Nu* variation, for correlating it with the variation of local *Re* calculated based on local T_f. Hence, the status of the correlation of the single-phase forced-flow convection in the laminar regime with *Br* has not been reported for the parameters obtained locally and along the flow. These form the motivation for the present study. This paper begins with a description of the experiment for studying the phenomenon from parameters obtained locally. The correlation of the experimental data with *Br* is verified, and the physical interpretation of the role of *Br* in spite of its relatively low values is elaborated.

2. Experimentation

The test section consists of two pieces of aluminum plates the dimensions of which are shown in Fig. 1 and Table 1. Table 2 gives D_h of the microchannels in specimens 1 (top) and 2 (bottom) for both the front and back of the specimens, from which $D_{h1} = 0.729 \pm 0.027$ and $D_{h2} = 0.727 \pm 0.023$ mm, where the uncertainties are the S.D. values, and measurements were made with an optical system. Table 3 gives the shortest distance between two consecutive microchannels,

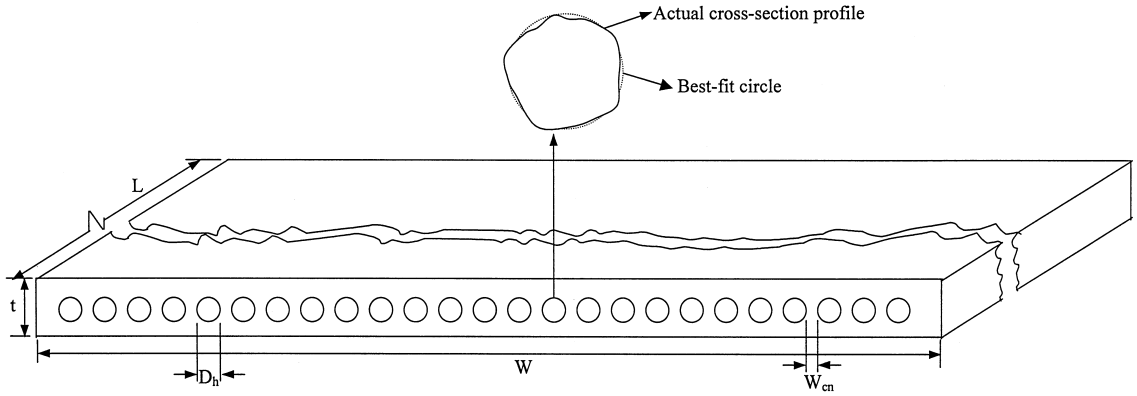

Fig. 1. Geometric details of microchannel test specimen.

Table 1
Geometric details of microchannel test specimens

No.	D_h (mm)	L (mm)	W (mm)	t (mm)	W_{cn} (mm)
1 (top)	0.729	115.5	30.5	1.414	1.244
2 (bottom)	0.727	116.2	30.5	1.417	1.246

Table 2
Idealised diameters of microchannels in specimens 1 and 2

No.	$D_{1,fr}$ (mm)	$D_{1,bk}$ (mm)	$D_{2,fr}$ (mm)	$D_{2,bk}$ (mm)
1	0.73822	0.73649	0.78256	0.71232
2	0.70995	0.71771	0.66708	0.70269
3	0.68447	0.72188	0.70356	0.70897
4	0.71448	0.72302	0.72568	0.71169
5	0.71438	0.73621	0.71721	0.72048
6	0.73128	0.73613	0.71729	0.71188
7	0.71522	0.75960	0.7215	0.72457
8	0.73316	0.75085	0.72506	0.73085
9	0.73288	0.75235	0.74Q9	0.73700
10	0.71866	0.75877	0.73857	0.73204
11	0.72015	0.77226	0.7383	0.74032
12	0.71769	0.77385	0.74207	0.78109
13	0.75160	0.78140	0.73028	0.76123
14	0.75263	0.75327	0.73202	0.75587
15	0.72779	0.75614	0.73814	0.75533
16	0.73700	0.74904	0.73264	0.73203
17	0.72986	0.74628	0.73427	0.73399
18	0.72827	0.75847	0.75763	0.73457
19	0.72885	0.75391	0.73555	0.73226
20	0.71265	0.75216	0.73171	0.73385
21	0.71054	0.74360	0.73433	0.71332
22	0.70737	0.72597	0.71289	0.73695
23	0.68361	0.70909	0.68470	0.70875
24	0.68980	0.69253	0.67203	0.70912
25	0.65113	0.65886	0.68757	0.70827
Mean	0.71767	0.74079	0.72414	0.72918
σ	0.02241	0.01848	0.02568	0.01926

$W_{cn1} = 1.244 \pm 0.017$ and $W_{cn2} = 1.247 \pm 0.013$ mm. Table 4 gives the thickness, t, of both specimens, measured by a pair of vernier calipers.

Fig. 2 shows the schematic of the experimental rig. On the left of the rig is a constant pressure head water tank with two valves mounted below. The water level in the tank is maintained constant by a constant supply of water from the main tap, and by ensuring that excess water is being drained from the tank. A beaker is used to collect the water from the outlet of the test section. A voltmeter (V), ammeter (A), and a variable transformer are mounted to the heater circuit as shown. The test specimens, with the strip heater sandwiched between them, are held tight by a retort stand. The heater supplies heat flux uniformly to the test specimens, simulating the constant wall heat flux boundary condition. Two pieces of perspex, one above and the other below the specimens, are held together by two G-cramps, and serve as insulation to prevent heat loss from the specimens to the ambient. Fig. 3 shows the top view of the layout of the thermocouple tips glued on the surface of specimen 1. As shown, the thermocouples are labeled from point 1 (15 mm from the left edge) to point 10, all other points being 10 mm apart. All the thermocouples are located on half the specimen width. A fast cure epoxy is used to secure the thermocouples to the walls of both specimens. The thermocouple junctions for specimen 2 are labeled from 11 (from the left edge of specimen 2) to 20. The thermocouple connectors are connected to the thermocouple selector. At the water inlet side (nearest to point 1 for the top specimen and point 11 for the bottom specimen), a thermocouple tip is inserted to measure $T_{f,in}$, and at the water outlet side, three thermocouples are inserted for measuring $T_{f,ex}$. The procedure to perform the experiment is summarised in Fig. 4. The maximum uncertainties of the experimentally derived quantities, obtained by a propagation of error analysis, are in Table 5.

Table 3
Shortest distance between consecutive microchannels in specimens 1 and 2

Distance between	$W_{cn,fr1}$ (mm)	$W_{cn,bk1}$ (mm)	$W_{cn,fr2}$ (mm)	$W_{cn,bk2}$ (mm)
1–2	1.23085	1.23170	1.23770	1.26233
2–3	1.25449	1.24005	1.24653	1.24479
3–4	1.27262	1.24345	1.24310	1.24445
4–5	1.23448	1.24557	1.23693	1.24605
5–6	1.24074	1.26044	1.25590	1.25250
6–7	1.24917	1.24881	1.26333	1.25807
7–8	1.24912	1.24387	1.25421	1.24079
8–9	1.24959	1.24643	1.24694	1.23958
9–10	1.24424	1.24895	1.23855	1.25168
10–11	1.25928	1.25882	1.24880	1.25482
11–12	1.24764	1.24276	1.25640	1.23841
12–13	1.25401	1.24990	1.24408	1.25934
13–14	1.25539	1.24945	1.25438	1.25490
14–15	1.23053	1.25011	1.25789	1.25406
15–16	1.25736	1.25549	1.24789	1.24471
16–17	1.25503	1.24573	1.24632	1.25156
17–18	1.24593	1.24933	1.25702	1.23541
18–19	1.24238	1.23200	1.24923	1.25496
19–20	1.25915	1.27348	1.24280	1.25237
20–21	1.23590	1.24006	1.26801	1.25332
21–22	1.23768	1.24110	1.22540	1.23283
22–23	1.25754	1.22176	1.23711	1.24322
23–24	1.23056	1.24408	1.25587	1.24731
24–25	1.17690	1.18517	1.20113	1.20295
Mean	1.24461	1.24369	1.24648	1.24668
σ	0.01799	0.01044	0.01360	0.00788

3. Analysis of experimental data

3.1. Processing of data

Table 6 gives the processed data for four cases of different V_m, $T_{f,in}$, and $T_{f,ex}$. The first column gives the axial location, x, on the microchannel specimen. The second gives T_w measured at axial location x. The next gives local T_f, calculated by linear interpolation from $T_{f,in}$, and $T_{f,ex}$, since the boundary condition is of the type, $\dot{q}''_w =$ constant. The next shows the local $\Delta T(x)$ $\{= T_w(x) - T_f(x)\}$. The fifth gives the coolant kinematic viscosity, ν, calculated by interpolation from T_f, from properties of saturated water in Ref. [12]. The sixth displays Re, calculated from ν, V_m, and D_h. The seventh gives local h, calculated from local ΔT as

$$h(x) = \dot{q}''_w/\Delta T(x). \tag{3}$$

The next column gives local Nu, calculated from $h(x)$. The next column gives Pr, calculated by interpolation using the table of properties in Ref. [12]. The next column gives Br, calculated from the coolant dynamic viscosity, μ, thermal conductivity, k, (both obtained by interpolation from Ref. [12]), V_m, and ΔT. The last column shows the parameter, $Nu/(Re^{0.62} \times Pr^{1/3})$. The constant wall heat flux supplied to the water is obtained as

Table 4
Thickness of microchannel specimen plates

No.	1	2	3	4	5	6	7	8	9
t_1 at different locations[a] (mm)	1.411	1.418	1.389	1.419	1.429	1.401	1.430	1.401	1.429
t_2 at different locations[b] (mm)	1.400	1.421	1.409	1.409	1.438	1.429	1.424	1.399	1.420

[a] $t_1 = 1.41411 \pm 0.01466$ mm.
[b] $t_2 = 1.41656 \pm 0.01322$ mm.

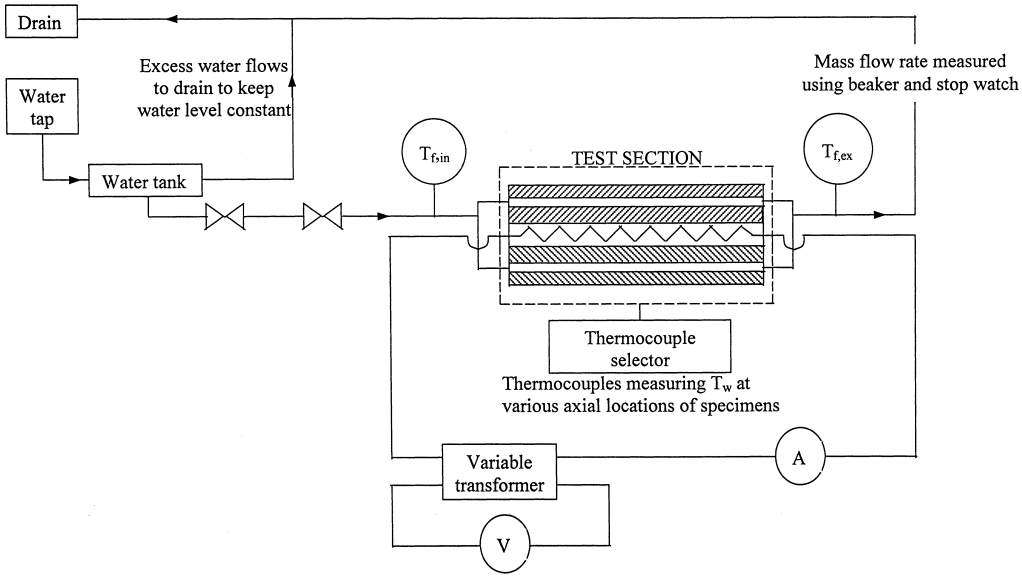

Fig. 2. Schematic of experimental rig.

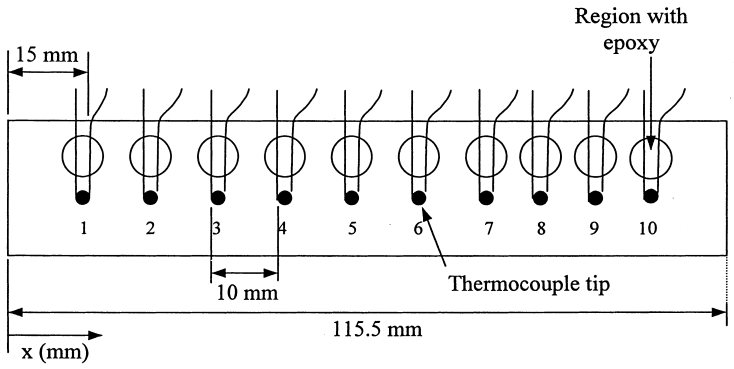

Fig. 3. Top view of layout of thermocouples on top specimen.

$$\dot{q}''_w = \frac{\dot{m} \times C_p \times (T_{f,ex} - T_{f,in})}{25\pi \times (D_{h,m1} \times L_{m1} + D_{h,m2} \times L_{m2})}, \quad (4)$$

where the denominator in Eq. (4) is the wetted area of all the microchannels in the specimens. Since $\dot{q}''_w$ has been determined from an enthalpy balance, the effect of axial conduction in the specimens need not be addressed. The C_p in Eq. (4) is evaluated at $(T_{f,in} + T_{f,ex})/2$.

Table 5
Typical uncertainties of parameters obtained from experiments

Parameter	$\dot{m}$	$\dot{q}''_w$	h	V	Nu	Re	Br
Uncertainty	1.2	3.2	6.1	13.8	9.2	15.5	28.4

The laminar data points are identified from Table 6 by observing the trend of Nu variation with Re. As reported in Refs. [5,6], the Nu decreases with increasing Re in the laminar regime. The variation of Nu with Re for the laminar data points, identified from the present experimental data, is shown in Fig. 5. All these data points are for a fully-developed flow, as shown in Fig. 4b [11]. For these data, the plot of the parameter $Nu/(Re^{0.62} \times Pr^{1/3})$ versus Br on a log–log scale is shown in Fig. 6, for the individual sets and also for

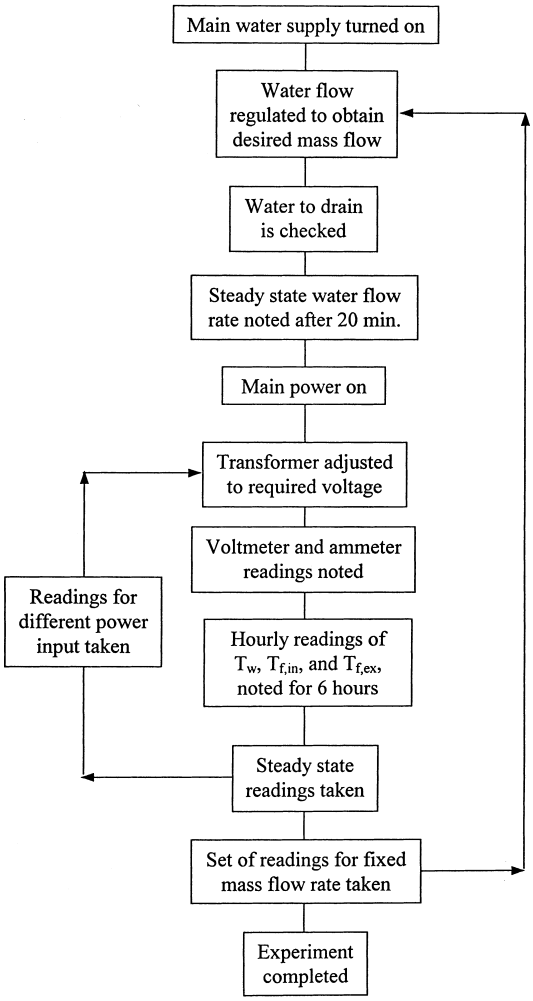

Fig. 4. Flow chart summarising experimental procedure.

the global set (combined data, shown by dashed line). As seen, the trend is a straight line for each of the individual data sets, supporting the correlation of the laminar forced-flow convection with *Br*, in addition to *Re* and *Pr*. Since only one geometric configuration is under investigation, the dimensionless geometric parameter in the convective heat transfer correlation is not being analysed. Interestingly, it is observed that the best linear fit for the combined data correlates much better quantitatively with the global data, than the best combined fit in Fig. 2a in Ref. [9], which uses data reported in Ref. [5]. This difference in the quality of the global best fits is attributed to the difference in the approach for obtaining the heat transfer and flow parameters, viz., *Nu*, *Re*, and *Pr*. In the literature [1,4,5–7], one parameter was obtained for the complete test-section. The variation of the parameter for fixed V_m was simulated by varying $\dot{q}''_w$, as in Refs. [5,6]. However, in the present approach, the constant $\dot{q}''_w$ boundary condition is simulated.

Table 7 gives the slopes and intercepts of the correlation of the parameter $Nu/(Re^{0.62} \times Pr^{1/3})$ with *Br* for the experimental data plotted on a log–log scale. The slope gives the exponent of *Br* in the correlation, and the intercept includes the logarithm of the dimensionless geometric function of the microchannels in the correlation. The exponent for the combined best fit is 0.64, which is within the range of the exponents for the four individual cases (0.56–0.73), and all the data points follow a unique trend. Hence, for the present experimental data, the global best fit agrees quantitatively and qualitatively with the individual best fits. However, the exponent for the combined best fit for the same correlation in Ref. [9] is an order of magnitude lower than for the three individual cases, presented in Table 5 [9] (exponent is 0.01, as compared to range 0.16–0.35), though the qualitative trend of the best fit is the same as that for the individual sets. However, for the experimental data reported in literature, some of the data points follow a trend opposite to that of the proposed correlation, as in Refs. [4,7]. Comparing the uncertainties in Table 7 with those in Table 5 [9], it is seen that the uncertainties in the correlation with *Br* are generally lower in the present case for the individual data sets, and more so for the global correlation. Hence, a universal correlation with *Br* can be obtained for different velocities, if the experimental data is obtained locally along the flow for the constant $\dot{q}''_w$ boundary condition.

The average convective transfer coefficients obtained from the present experimental data using Eqs. (1), (2) and (5) (given below), are in Table 8, where the average has been obtained for the length over which the flow is laminar. The quantities in the bracket give the percentage error with reference to the average obtained by

$$\bar{h} = \frac{\int_0^{L_{lm}} h(x)\,dx}{L_{lm}}, \tag{5}$$

where $h(x)$ is the present laminar experimental data, obtained from Eq. (3). Generally, the values obtained from Eq. (1) are lower, since the wall–fluid temperature difference also includes the temperature change of the fluid from the inlet to the downstream end of the microchannel, in addition to the local wall–fluid temperature difference, $\Delta T(x)$, though it provides a representative heat transfer coefficient for the entire test specimen. However, the qualitative trends of the average *h* values obtained using the three different approaches are identical. Hence, the behaviour of *Nu* with *Re* does not change by changing the definition of the average convective heat transfer coefficient.

Table 6
Processed data from experiments

x (mm)	T_w (°C)	T_f (°C)	ΔT (K)	$\nu \times 10^7$ (m^2/s)	Re	h (W/m^2 K)	Nu	Pr	$Br \times 10^8$	$[Nu \times (Re^{0.62} \times Pr^{1/3})]^{-1} \times 100$
(a) Case 1: $-V_m = 1.33$ cm/s, $\dot{q}''_w = 4527.7$ W/m^2, $T_{f,in} = 28.0$°C, $T_{f,ex} = 68.2$°C										
15	44.8	33.2	11.6	7.552	12.8	301.8	0.3543	5.05	1.8144	4.260
25	48.9	36.7	12.2	7.039	13.7	287.0	0.3338	4.6	1.5918	3.949
35	52.7	40.2	12.5	6.591	14.6	280.1	0.3236	4.3	1.4429	3.766
45	56.8	43.7	13.1	6.192	15.6	267.2	0.3068	4.0	1.2811	3.514
55	60.8	47.1	13.7	5.818	16.6	255.6	0.2914	3.7	1.1445	3.290
65	63.7	50.6	13.1	5.503	17.5	267.3	0.3031	3.5	1.1195	3.375
75	66.5	54.1	12.4	5.188	18.6	282.3	0.3159	3.2	1.1017	3.475
85	69.4	57.6	11.8	4.931	19.6	296.7	0.3299	3.0	1.0902	3.585
95	71.2	61.1	10.1	4.684	20.6	346.6	0.3838	2.9	1.2023	4.115
105	72.6	64.5	8.1	4.452	21.7	432.2	0.4752	2.7	1.4141	5.038
(b) Case 2: $-V_m = 1.83$ cm/s, $\dot{q}''_w = 5450.3$ W/m^2, $T_{f,in} = 27.2$°C, $T_{f,ex} = 56.5$°C										
15	41.8	31.0	10.8	7.904	16.7	323.4	0.3816	5.31	3.8553	3.815
25	46.1	33.5	12.6	7.508	17.6	277.2	0.3251	5.01	3.1198	3.209
35	49.0	36.1	12.9	7.132	18.5	270.7	0.3154	4.73	2.8707	3.077
45	53.5	38.6	14.9	6.793	19.5	234.4	0.2716	4.47	2.3544	2.618
55	56.2	41.2	15.0	6.468	20.4	232.8	0.2685	4.23	2.2124	2.558
65	57.5	43.7	13.8	6.187	21.4	253.1	0.2905	4.03	2.2866	2.737
75	59.3	46.3	13.0	5.912	22.4	268.7	0.3068	3.82	2.3048	2.857
85	61.6	48.8	12.8	5.664	23.4	272.9	0.3104	3.64	2.2308	2.859
95	63.3	51.3	12.0	5.418	24.4	291.0	0.3298	3.47	2.2665	3.006
105	64.3	53.9	10.4	5.203	25.4	335.8	0.3790	3.32	2.4990	3.421
(c) Case 3: $-V_m = 2.71$ cm/s, $\dot{q}''_w = 8144.9$ W/m^2, $T_{f,ex} = 27.9$°C, $T_{f,ex} = 73.9$°C										
15	38.9	33.9	5.0	7.446	26.3	1629.0	1.9086	4.97	17.082	14.75
25	43.7	37.9	5.8	6.893	28.4	1404.3	1.6296	4.54	13.454	12.36
35	47.7	41.8	5.9	6.387	30.6	1380.5	1.5901	4.18	12.170	11.84
45	52.3	45.8	6.5	5.962	32.8	1253.1	1.4325	3.86	10.209	10.48
55	57.8	49.8	8.0	5.558	35.2	1018.1	1.1562	3.57	7.6757	8.317
65	62.4	53.8	8.6	5.211	37.5	947.1	1.0689	3.32	6.6364	7.567
75	65.3	57.8	7.5	4.914	39.8	1086.0	1.2178	3.11	7.1091	8.499
85	69.1	61.8	7.3	4.631	42.3	1115.7	1.2421	2.90	6.8183	8.544
95	72.7	65.7	7.0	4.368	44.7	1163.6	1.2890	2.72	6.6734	8.745
105	74.1	69.7	4.4	4.116	47.4	1851.1	2.0341	2.54	9.9089	13.615
(d) Case 4: $-V_m = 2.43$ cm/s, $\dot{q}''_w = 7446.7$ W/m^2, $T_{f,in} = 28.4$°C, $T_{f,ex} = 75.4$°C										
15	39.6	34.5	5.1	7.362	23.8	1460.2	1.7082	4.90	13.249	14.09
25	44.6	38.6	6.0	6.804	25.8	1241.1	1.4383	4.47	10.280	11.64
35	48.8	42.6	6.2	6.301	27.8	1205.0	1.3859	4.11	9.1706	11.01
45	53.5	46.7	6.8	5.868	29.9	1095.1	1.2498	3.79	7.6840	9.756
55	59.6	50.8	8.8	5.466	32.1	846.2	0.9595	3.51	5.4877	7.359
65	63.9	54.9	9.0	5.133	34.2	827.4	0.9323	3.26	4.9922	7.039
75	67.7	58.9	8.8	4.832	36.3	846.2	0.9470	3.05	4.7697	7.050
85	71.7	63.0	8.7	4.548	38.5	855.9	0.9513	2.85	4.4998	6.979
95	75.0	67.1	7.9	4.281	40.9	942.6	1.0423	2.66	4.6318	7.533
105	76.7	71.1	5.6	4.043	43.4	1329.8	1.4563	2.48	6.0888	10.389

3.2. Physical interpretation of role of Br in microchannels

From Table 6, it is seen that the values of Br are relatively very small (of the order of 10^{-8}). Hence, the laminar single-phase convection correlates with Br in microchannels in spite of these relatively low values of Br. The values of Br obtained from the present experiments are too low to affect T_f directly due to viscous dissipation, discussed for instance by White [13], and Shah and Bhatti [14]. Hence, the effect of Br is at the temperature gradient level, since for low values it can-

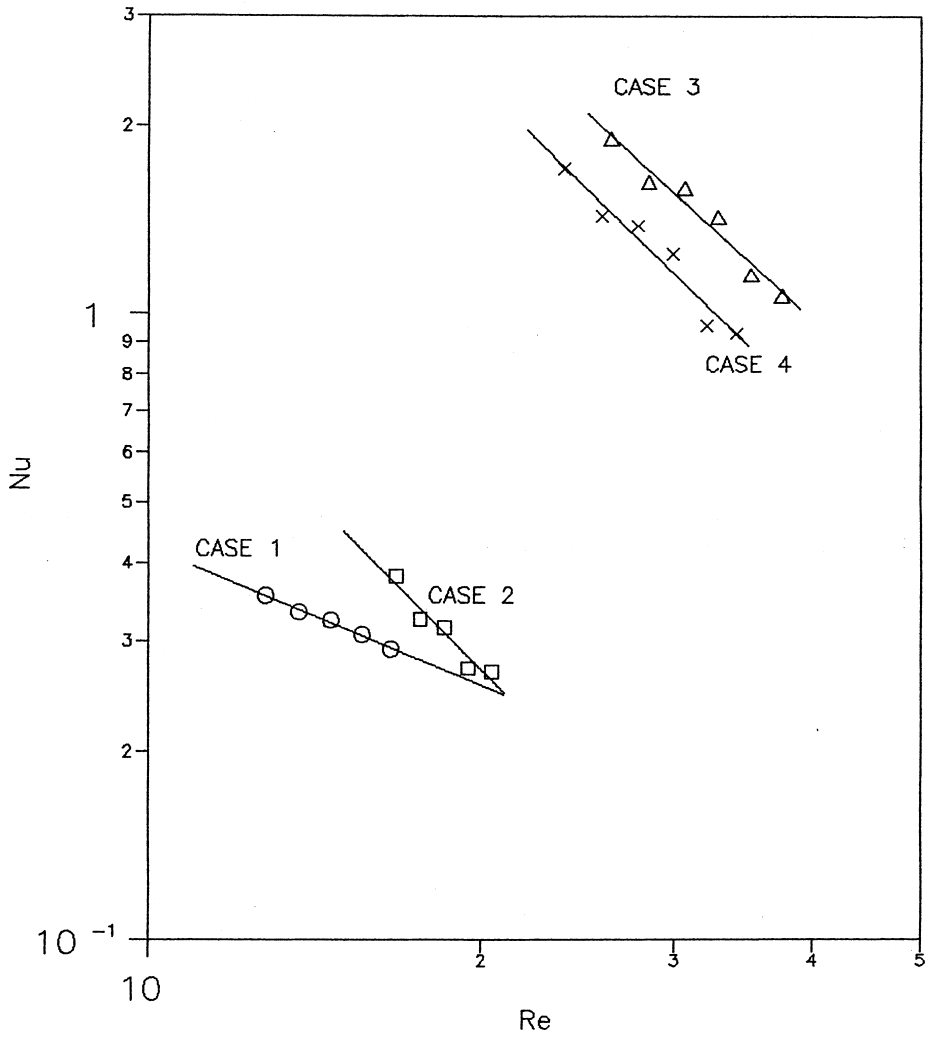

Fig. 5. Plot of *Nu* vs. *Re* for four cases in Table 6.

not directly affect T_f. From Table 6 and Fig. 6, *Br* is seen to change along the flow. As seen, *Br* reduces at the exit by about 50% of its value close to the inlet, mainly because of the reduction in μ, due to increase in T_f, and due to an associated increase in ΔT. Hence, changes in *Br* along the flow affect the temperature gradient along the flow, which has been mentioned in Ref. [9]. Since the ratio of the fluid temperature gradient at the wall and the wall–fluid temperature difference determines *h*, variations in *Br* affect the convective heat transfer in microchannels. In the conventionally-sized channels, the variation of *Br* due to

Table 7
Slopes and intercepts of correlations and their uncertainties for data in Table 6

Case	Slope	σ_{slope}	Intercept	$\sigma_{intercept}$
1	0.56	0.01	2.94	0.06
2	0.73	0.02	4.0	0.2
3	0.71	0.02	4.0	0.1
4	0.72	0.02	4.1	0.1
Combined	0.64	0.06	3.5	0.4

Table 8
Convective heat transfer coefficients in, W/m^2 K, for four cases in Table 6

Eq. No.	Case 1 (%)	Case 2 (%)	Case 3 (%)	Case 4 (%)
1	138.0 (50.8)	187.9 (31.0)	236.1 (81.8)	209.8 (81.6)
2	358.7 (27.9)	426.3 (56.6)	1227.0 (5.6)	1084.5 (4.8)
5	280.5	272.3	1299.5	1139.2

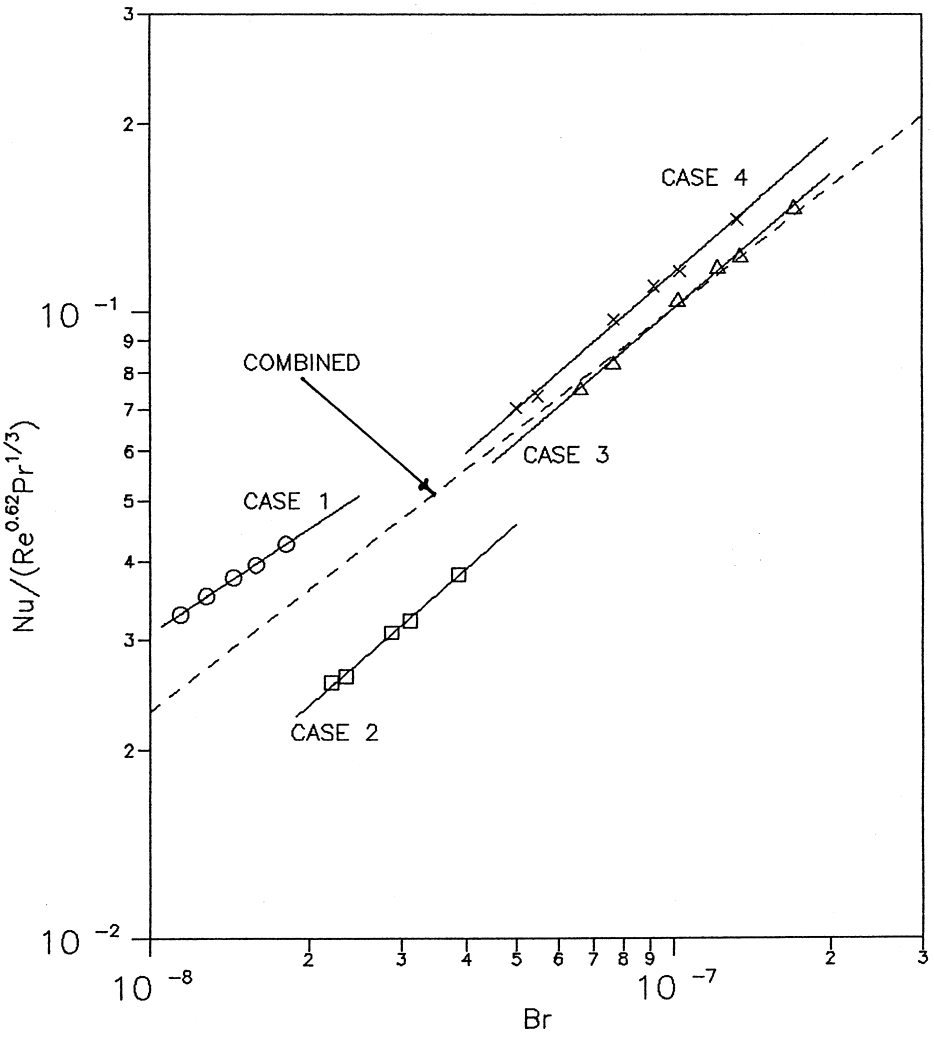

Fig. 6. Plot of $Nu \times (Re^{0.62} \times Pr^{1/3})^{-1}$ vs. Br for four cases in Table 6

variation of μ is generally negligible, mainly because the gradients are not steep. Hence, for a fully-developed flow for the constant wall heat flux boundary condition, Nu is constant {=4.364, as mentioned, for instance, in Eq. (26) of Ref. [15]}. Hence, ΔT = constant when the flow is fully-developed. However, in microchannels, ΔT increases along the flow even after the flow is fully-developed, as seen from Fig. 5 [11]. Hence, in microchannels, the temperature gradient and ΔT change along the flow, i.e. the temperature profile changes for a fully-developed flow, and these variations in the temperature profile along the flow are captured by the variations in Br along the flow. This effect of variations in Br in microchannels due to variation in coolant properties, and which affects the single-phase convective heat transfer at the temperature gradient level, is identified here as the *secondary effect of Br*. When Br is large (of the order of unity or higher), it affects T_f directly due to the effect of viscous dissipation, even for a constant value of Br along the flow, and this effect will now be termed the *primary effect of Br*. This primary effect has been extensively discussed in the literature, and is applicable to both conventionally-sized channels and microchannels.

The temperature and velocity gradients in microchannels are steep and well-maintained in the laminar regime. The steep temperature gradient over the cross-section (which increases with the amount of heat transfer) causes the viscosity to vary substantially over the cross-section. The distortion of the laminar velocity profiles due to variation of viscosity over the cross-section as a result of heating or cooling has been qualitatively compared with the parabolic velocity profile by Kays and Perkins [15] in their Fig. 99. Furthermore,

the temperature gradient along the flow (which also increases with the amount of heat transfer) changes the bulk coolant viscosity along the flow. It is noteworthy that both the axial and cross-sectional variations in T_f are captured by variations in *Br*. The axial variations in T_f are captured by the variations in the bulk viscosity μ, and the variation in the viscosity change over the cross-section is captured by variations in ΔT. Hence, for heat transfer in microchannels, the velocity profile will change along the flow even when it is fully-developed, though V_m still remains constant along a steady and incompressible flow. Since the velocity profile dictates the velocity gradient and hence the frictional loss, the flow friction models for microchannels proposed in the literature without considering heat transfer [4,7,8,16–18] must be re-examined for their applicability with heat transfer.

The effect of variation of viscosity due to heat transfer causes a coupling between the velocity and temperature fields, discussed, for instance, in [13]. The variation of velocity profile along the flow is due to variation of pressure gradient, which is captured by the '$\mu \times V_m^2$' in *Br*. In addition, steep axial variations in T_f will cause axial variations in the velocity and temperature profiles, also mentioned in Ref. [13]. Thus, strictly speaking, there is never a fully-developed regime in microchannels. The coupling is strong when the variation of viscosity along and across the cross-section is steep. This happens especially in microchannels with heat transfer due to the small dimensions and hence the small heat capacity of the coolant associated with its small mass in flow through microchannels. The *Br* not only captures the variation of viscosity along and across the cross-section, but also the coupling between momentum transfer (represented by '$\mu \times V_m^2$') and conduction heat transfer (represented by '$k \times \Delta T$') across the flow, because of these variations. This physical significance of *Br* is elaborated in Ref. [9].

3.3. Verification of role of Br in flow transition

The *Re* and *Br* at the laminar-to-transition change are identified from the change in the trend of *Nu* versus *Re*,, as discussed earlier, based on the known unusual behaviour, and are presented in Table 9. These transition points are plotted on a log–log scale in Fig. 7. These points follow a linear relationship, thereby supporting the earlier proposed form of correlating the transition points (Eq. (2.1) [10]). Hence, *Br* plays a role in determining the flow transition points even when experimental data is obtained locally along the flow.

The *Br* plays a role in determining the flow regime boundaries only with heat transfer, due to the variation of profiles along and across the flow, as discussed in [10]. Without heat transfer, the flow regime boundaries are solely determined by *Re*. The Re_{tr} reduces with the microchannel dimensions, as reported for instance in Refs. [4,7].

4. Conclusions

1. The single-phase forced convective heat transfer in the laminar regime in microchannels correlates with the Brinkman number even when the experimental data is obtained locally and along the flow, for the constant wall heat flux boundary condition.
2. The global correlation with *Br* is much better in trend and especially quantitatively, for the constant wall heat flux boundary condition, for which data is obtained along the flow.
3. Universal correlation of convective heat transfer with *Br* can be obtained for the constant wall heat flux boundary condition, and the data points obtained locally along the flow.
4. The Brinkman number correlates the convection in spite of its relatively low values.
5. Variations in the Brinkman number capture the variation in the change in viscosity over the cross-section and the variation in viscosity along the flow, and the momentum transfer and conduction heat transfer across the flow.
6. The viscosity variations couple the temperature and velocity fields, causing a change in the temperature profile along and across the flow, which affect the convection. This effect generally observed in microchannels is identified here as the secondary effect of *Br*.
7. The *Br* plays a role in determining the flow transition points even when experimental data is obtained locally along the flow for the constant wall heat flux boundary condition.

Table 9
Flow transition points identified from Table 6

Case	1	2	3	4
Re_{tr}; Br_{tr}	16.6; 1.1445×10^{-8}	20.4; 2.2124×10^{-8}	34.2; 4.9922×10^{-8}	37.5; 6.6364×10^{-8}

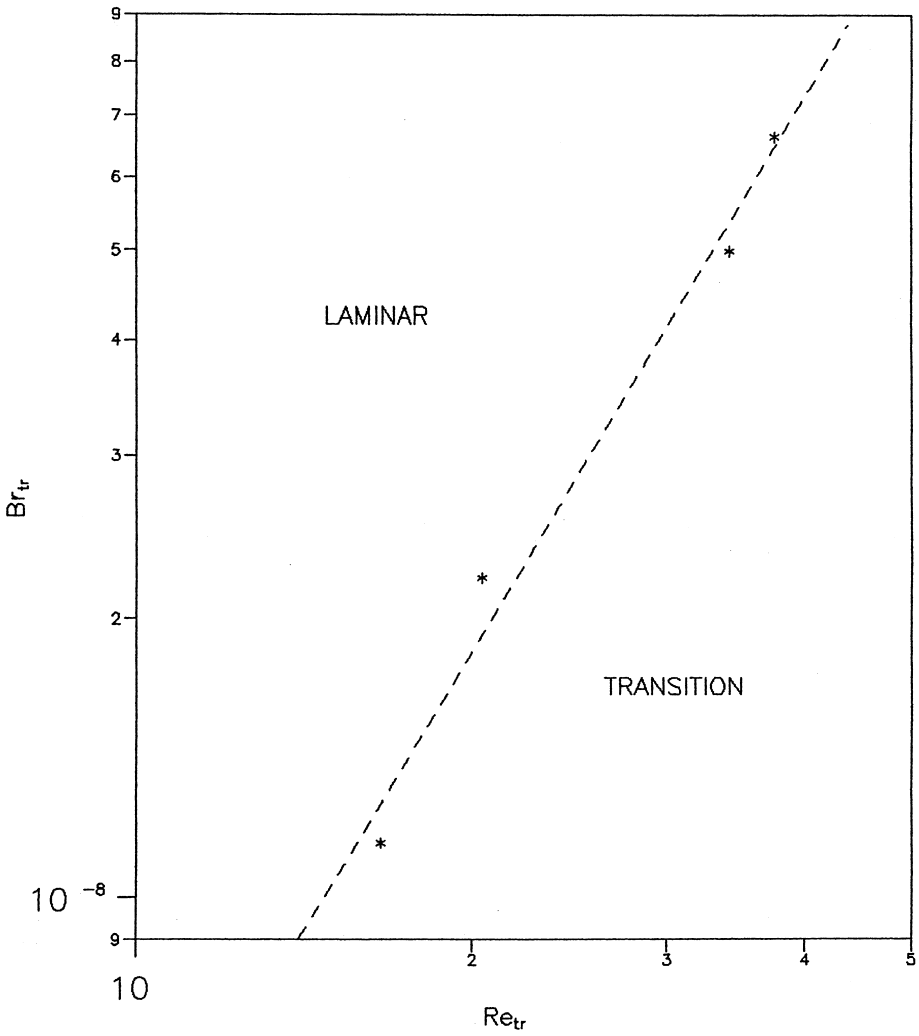

Fig. 7. Locus of laminar-to-transition change points for experimental data.

Acknowledgements

The authors gratefully acknowledge the support provided by the National Science and Technology Board of Singapore, project number JTARC 5/96, and the assistance of Y.S. Tan in the experiment.

References

[1] X.F. Peng, B.X. Wang, Forced convection and flow boiling heat transfer for liquid flowing through microchannels, International Journal of Heat and Mass Transfer 36 (14) (1993) 3421–3427.
[2] E.N. Sieder, G.E. Tate, Heat transfer and pressure drop of liquids in tubes, Industrial Engineering and Chemistry 28 (1936) 1429–1435.
[3] P.Y. Wu, W.A. Little, Measurement of friction factor for the flow of gases in very fine channels used for microminiature Joule–Thompson refrigerators, Cryogenics 23 (5) (1983) 273–277.
[4] X.F. Peng, G.P. Peterson, B.X. Wang, Heat transfer characteristics of water flowing through microchannels, Experimental Heat Transfer 7 (1994) 265–283.
[5] B.X. Wang, X.F. Peng, Experimental investigation on liquid forced-convection heat transfer through microchannels, International Journal of Heat and Mass Transfer 36 (Suppl. 1) (1994) 73–82.
[6] X.F. Peng, G.P. Peterson, The effect of thermofluid and geometrical parameters on convection of liquids through rectangular microchannels, International Journal of Heat and Mass Transfer 38 (4) (1995) 755–758.
[7] X.F. Peng, G.P. Peterson, Convective heat transfer and flow friction for water flow in microchannel structures, International Journal of Heat and Mass Transfer 39 (1996) 2599–2608.
[8] G.M. Mala, D. Li, J.D. Dale, Heat transfer and fluid

flow in microchannels, International Journal of Heat and Mass Transfer 40 (1997) 3079–3088.

[9] C.P. Tso, S.P. Mahulikar, The use of the Brinkman number for single phase forced convective heat transfer in microchannels, International Journal of Heat and Mass Transfer 41 (12) (1998) 1759–1769.

[10] C.P. Tso, S.P. Mahulikar, The role of the Brinkman number in analysing flow transitions in microchannels, International Journal of Heat and Mass Transfer 42 (1999) 1813–1833.

[11] C.P. Tso, S.P. Mahulikar, Proceedings of 2nd IEEE Electronics Packaging Technology Conference, 8–10 December, Singapore, 1998, pp. 126–132.

[12] J.P. Holman, in: Heat Transfer, 7th ed., McGraw-Hill, London, 1990, p. 663.

[13] F.M. White, Viscous Fluid Flow, 2nd ed., McGraw-Hill, New York, 1991.

[14] R.K. Shah, M.S. Bhatti, Laminar convective heat transfer in ducts, in: S. Kakac, R.K. Shah, W. Aung (Eds.), Handbook of Single-Phase Convective Heat Transfer, John Wiley and Sons, New York, 1987, pp. 3–12.

[15] W.M. Kays, H.C. Perkins, Forced convection, internal flow in ducts, in: W.M. Rohsenow, J.P. Hartnett E.N. Ganic (Eds.), Handbook of Heat Transfer Fundamentals, 2nd ed., McGraw-Hill, New York, 1985, pp. 7-130–7-132.

[16] S.B. Choi, R.F. Barron, R.O. Warrington, Fluid flow and heat transfer in microtubes, ASME — Micromechanical Sensors, Actuators, and Systems 32 (1991) 123–134.

[17] M.M. Rahman, F. Gui, Experimental measurements of fluid flow and heat transfer in microchannel cooling passages in a chip substrate, ASME — Advances in Electronic Packaging 4-2 (1993) 685–692.

[18] X.F. Peng, G.P. Peterson, B.X. Wang, Frictional flow characteristics of water flowing through rectangular microchannels, Experimental Heat Transfer 7 (4) (1994) 249–264.